NUCL SCI TECH (2016) 27:125
DOI 10.1007/s41365-016-0121-7

Quantitative analysis of 3D vasculature for evaluation of angiogenesis in liver fibrosis with SR-μCT

Hai Tan[1,2] · Yi Fu[3,4] · Da-Dong Wang[5] · Xi Zhang[3,4] · Ti-Qiao Xiao[1,2]

Received: 10 April 2016 / Revised: 12 July 2016 / Accepted: 17 July 2016 / Published online: 3 September 2016

Abstract The micro-CT imaging of vasculature is a powerful tool for evaluation of angiogenesis, a prominent characteristic of hepatic fibrosis. The segment or bifurcation density, which is usually adopted to evaluate the degree of hepatic fibrosis, does not always work and may lead to incorrect assessment, especially when the three-dimensional vasculature obtained is imperfect in sample preparation or image collection. In this paper, we propose a new parameter to solve this problem. The experimental results demonstrate that the method is robust and reliable, and is practical for angiogenesis evaluation, despite of image data imperfections. This quantitative analysis method can be extended to investigate other kinds of diseases in which vasculature change is a key indicator.

Keywords SR-μCT imaging · 3D image processing · Quantitative analysis · 3D vasculature · Angiogenesis

1 Introduction

Nowadays, liver fibrosis and its end-stage, cirrhosis, become a major threat to the public's health. It occurs in many chronic hepatic diseases and may lead to severe complications [1, 2]. The evaluation of the hepatic fibrosis is critical in the diagnosis and treatment of such hepatic disease. Angiogenesis is one of the prominent characteristic of hepatic fibrosis [3, 4]. With the development of imaging techniques, particularly the synchrotron radiation-based micro-tomography (SR-μCT) [5], hepatic vasculature imaging and its quantification are widely used in studying the development of hepatic fibrosis [6, 7]. Phase-contrast imaging (PCI)-based SR-μCT is able to detect minute density variation between biological soft tissues, which allows inspection of vascular microstructures without contrast agent. However, three-dimensional images with elaborate hepatic vasculature introduce challenges to the structural analysis and extraction of quantitative information.

For quantification of angiogenesis to evaluate the fibrosis progression, a series of parameters should be extracted from the vasculature, such as micro-vessel density (MVD), the ratio of extreme vessel to volume (*E/V*) and the ratio of junction point to volume (*J/V*) [3, 4, 8, 9]. However, vessels in the liver do not distribute uniformly, so the density descriptors limit accurate assessment of angiogenesis. Due

Hai Tan and Yi Fu have contributed equally to this work.

This work is supported by the National Basic Research Program of China (No. 2010CB834301), CAS-CSIRO Collaborative Research Project (GJHZ1303), the Shanghai Municipal Natural Science Foundation (No. 11ZR1407800), and the Joint Funds of the National Natural Science Foundation of China (Nos. U1232205, 81430087 and 81271574).

✉ Xi Zhang
zhangxi0009@163.com

✉ Ti-Qiao Xiao
tqxiao@sinap.ac.cn

[1] Shanghai Institute of Applied Physics, Chinese Academy of Sciences, Jiading Campus, Shanghai 201800, China

[2] University of Chinese Academy of Sciences, Beijing 100049, China

[3] Department of Radiology, Cancer Hospital, Fudan University, Shanghai 200032, China

[4] Department of Oncology, Shanghai Medical College, Fudan University, Shanghai 200032, China

[5] Quantitative Imaging, CSIRO Data61, Marsfield, NSW 2122, Australia

to limitations in the sample preparation and the imaging, the intact vasculature in a specimen may not be imaged integrally and three dimensionally, which means that available parameters for angiogenesis assessment cannot ensure the accuracy and reliability. In this paper, based on the tree structure of hepatic vasculature, a quantification is introduced to assess the degree of angiogenesis. Experiments based on a series of collected and simulated liver specimens at different stages of fibrosis are performed to evaluate practicability of the proposed method.

2 Specimen preparation and image acquisition

2.1 Specimen preparation

All animal experiments were performed with approval of the Institutional Animal Care and Use Committee of Shanghai University of Medicine. Twenty-six experimental BALB/c mice (males, 5 weeks old, weighing 20–30 g) were maintained under specific pathogen-free conditions. Sterile solutions of thioacetamide dissolved in 0.9 % saline were intraperitoneal injected to induce liver fibrosis, administered twice weekly (40 mg/mL, 200 mg/kg body weight) for 8 weeks. In order to access the progression of fibrosis, two mice per time point were euthanized at the end of two injections, and a saline solution was injected into the portal vein to displace the blood. We excised the liver samples, fixed and embedded in 10 % formalin, and stained with haematoxylin and Masson's trichrome for liver fibrosis staging. The control group received just saline injections.

All pathological evaluations were made by two experimental pathologists according to the METAVIR score for standardization purposes [10]. Any discrepancies between the two observers were settled by consensus. The staging system consists of no fibrosis = $F0$; portal fibrosis without septa = $F1$; a few septa = $F2$; numerous septa without cirrhosis = $F3$; and cirrhosis = $F4$ [11]. Two subgroups were set up corresponding to mild fibrosis (including $F1$ and $F2$) and advanced fibrosis (including $F3$ and $F4$). SR-μCT images were reviewed independently by two radiologists with 6 and 8 years of experience, respectively. Both readers were blinded to all clinical and pathological findings.

2.2 Imaging by synchrotron radiation-based micro-tomography

Phase-contrast SR-μCT using propagation-based technique was used to capture images of the specimens at Beamline BL13W1 (SSRF, Shanghai, China) [12]. This imaging technique that utilizes phase shifts rather than absorption information greatly improves the density resolution, being able to image different regions of the sample where attenuation coefficient is too small to be detected.

The X-ray beam at 15 keV, from a double-crystal monochromator (Si111), was used in the experiments. X-ray photons transmitted through the specimen were detected by a detector (a scintillator plus a charge-coupled device), positioned at 70 cm downstream the sample. The image pixel size was 3.7 μm, and the field of view was 49.8 mm (H) × 5.04 mm (V). For each CT scan, 720 projections were taken at angles evenly distributed from 0° to 180°. Exposure time per project was 2 s. The total time of X-ray exposure was approximately 35 min. The sample holder was glued on stands adapted to the rotation stage. The rotation centre of the sample was positioned perpendicular to the X-ray beam. In the data collecting, 20 flat-field images (without sample in the X-ray) at every 40 projections were taken, and ten dark-field images (no X-ray beam hitting the detector) were recorded, which were used for image preprocessing to the projections.

2.3 Image reconstruction

All the image datasets are reconstructed by the software PITRE [13]. Phase retrieval was implemented to each projection image, and the stack image was reconstructed using the filtered back-projection algorithm. The output 32-bit stack images are converted to 8-bit so as to conduct further image processing and analysis. There are 8 stack images in total. Figure 1 shows the 3D rendering of all the reconstructed images, some of which miss a portion of the specimen so that the vasculature inside the liver is not intact.

3 Quantitative analysis to the vascular tree

In this section, we explain the method of tree analysis for the hepatic vasculature in details so that the acquired quantitative parameters are able to evaluate the degree of liver fibrosis efficiently. The procedures of acquiring quantitative information of the vasculatures from the micro-CT images are illustrated in Fig. 2.

3.1 Image preprocessing

Figure 3a is the raw image after CT reconstruction and image preprocessing. Figure 3b is the liver mask obtained by employing a Gaussian filtering to Fig. 3a with a high sigma value. The major outline of the liver is isolated from Fig. 3a using the liver mask, and Fig. 3d shows the image processed further by Ostu thresholding in which the vasculature and image background voxels are shown at the

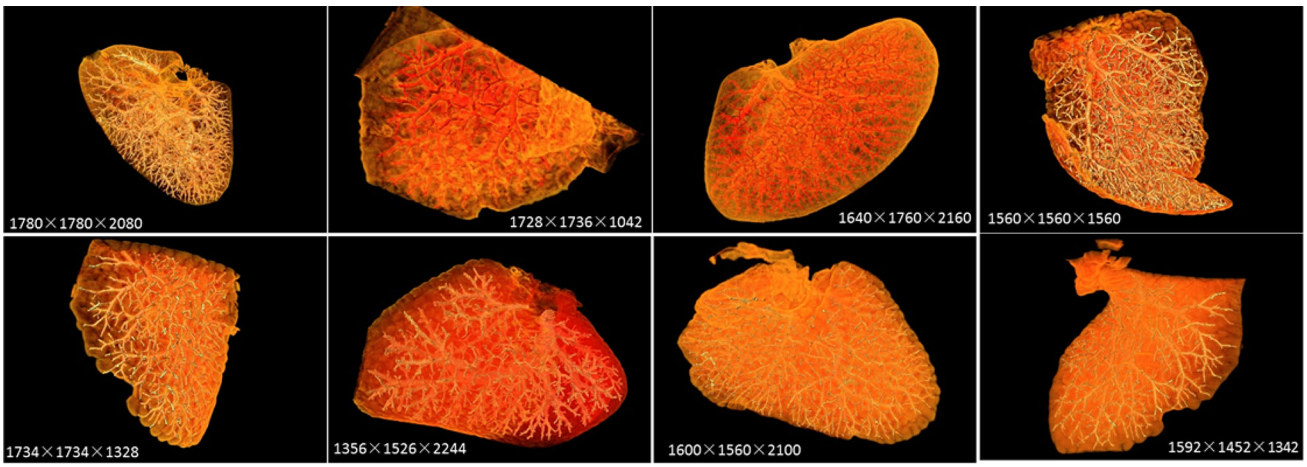

Fig. 1 Typical reconstructed images for eight pieces of mouse liver samples at different liver fibrosis stages

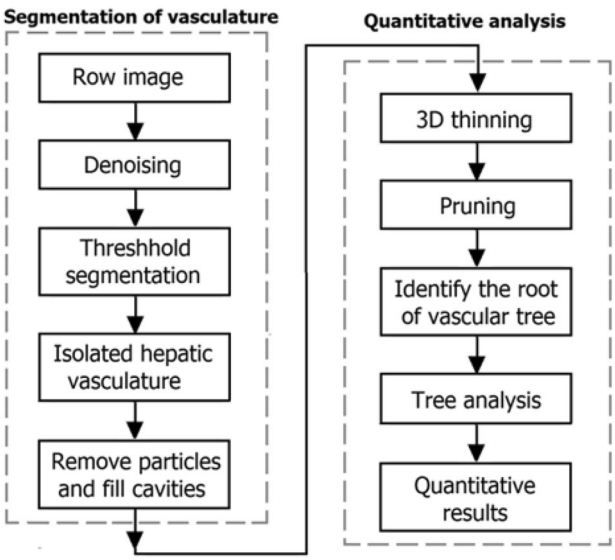

Fig. 2 Flowchart of tree analysis to the hepatic vasculature

same grey value. Figure 3e is a dedicated mask image used to isolate vasculature, which is generated by the convex hull of the liver shape in Fig. 3c and used for morphological 3D erosion to confine the vasculature out of the background if necessary. After all these procedures, the slice image of the isolated vasculature is achieved (Fig. 3f).

The particle-removing and cavity-filling procedures are as follows.

Cavity is a region where grey values of all voxels are 0, and it is surrounded by object voxels. There is only one background component in an image. All the cavities are filled once the only background component is segmented by region-growing method. Then, the grey value of the whole 3D image is inversed.

All the object components are labelled and counted by ImageJ plugin "3D Objects Counter" [14]. The components of smaller sizes than a threshold are removed. And the binary image containing the solid vasculature is ready for further quantification.

3.2 Generating vascular skeleton

3.2.1 Skeletonization

Generally, skeletonization is an efficient approach to analyse the vasculature, because the structural parameters such as the vessel length, the number of vessel segments, and the number of bifurcations are effectively conveyed in curve skeleton, a "compact" representation. A vascular skeleton used for quantitative analysis should focus on some properties [15] of this linear structure, such as homotopic, thinness, centeredness, computational efficiency. Particularly, the hierarchic feature of skeleton plays an important role in the tree structure analysis of vasculature. The LKC skeletonization algorithm [16, 17], which preserve well the topology of the vessels, is exploited to the segmented vasculature to generate the vascular skeleton.

3.2.2 Pruning

The skeleton is intrinsically sensitive to small changes at the object's boundary. Therefore, the resulted skeleton may contain many spurious branches which are the erroneous representation of the vascular branches. Pruning [18] is a common solution to remove the spurious branches by eliminating short terminal branches smaller than a threshold.

3.3 Quantification and vascular tree analysis

The segmented vasculature and its associated skeleton are prepared to extract the statistical information of the

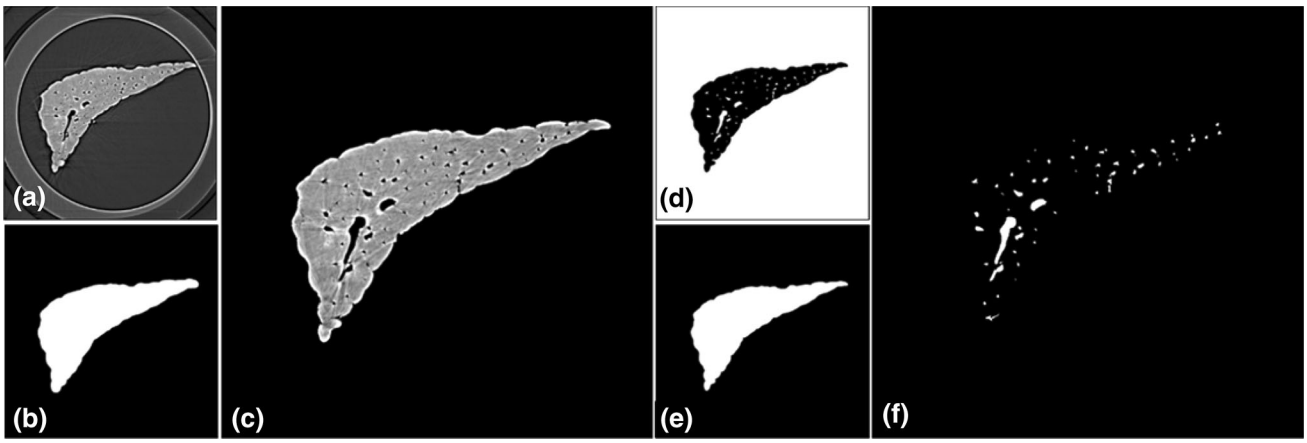

Fig. 3 Procedures for isolating vasculature from background

vasculature based on its tree structure. This section describes the quantitative analysis of hepatic vasculature in details. We highlight the analysis of the characteristics of the vascular tree, whose output contains the geometry information of each vascular branch in hierarchy.

3.3.1 The root of vascular tree

This is the start position for tracing the whole tree structure of vasculature. The root is identified automatically. We scan each slice from the first frame to the last one along six directions of the axes in the 3D image space $Z^3(\pm X, \pm Y, \pm Z)$. In the first frame every object voxel is searched, the largest and central connected region in the 2D frame is selected as the candidate root area. Therefore, there are six candidate root regions in terms of the six scanning directions. Then, we calculate the largest inscribed sphere inside the vasculature to obtain the approximate location of the root. The candidate root area being the closest to the largest inscribed sphere is considered as the reference root. If a 3D image has more than one vascular tree, we could label all the connected components to differentiate all trees and identify trees' roots based on the tree labels. Besides, the manually specified root can also be accepted if this is preferred.

3.3.2 Elements of the vasculature

The 3D vascular tree analysis method is developed from the 2D image analysis of neurite outgrowth [19]. This method outputs quantitative information of the vascular trees on both statistics and tree hierarchy images.

Figure 4 illustrates the tree structure of vasculature. The r_1, s_{1-8}, b_{1-3} and e_{1-4} are the root, branches, bifurcations and extremities, respectively. Table 1 lists definitions of the elements in a vascular tree, and the serial properties concerning measurements and structure information.

The following values are given to r_1, s_2, b_3 and e_4 in Fig. 4.

r_1: $RL(r_1) = 1$, $RST(r_1) = s_1$
s_2: $VL(s_2) = 2$; $VLen(s_2) =$ length of s_2; $VRad(s_2) =$ radius of s_2; $VLV(s_2) = 2$; $VR(s_2) = r_1$; $VP(s_2) = b_1, b_2$; $VT(s_2) =$ sub-tree 1
b_3: $BL(b_3) = 3$: $BV(b_j) = s_3, s_6, s_7, s_8$
e_4: $EL(e_4) = 4$. $ELR(e_4) = VLen(s_1) + VLen(s_3) + VLen(s_7)$, $EB(e_4) = s_7$

Then, the vasculature quantification is to traverse the vascular tree and assign property values to each element.

3.3.3 Traversing vascular tree and the related measurement

There are several preprocessing workflows before constructing the vasculature tree. Firstly, a label is given to each root of vascular tree. Next, the skeleton of vasculature is divided into unique vessel segment, by removing the intersection voxel from the skeleton. An intersection point

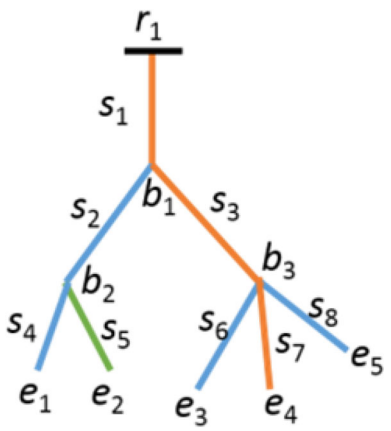

Fig. 4 Tree structure of vasculature

Table 1 Elements in a vascular tree and the serial properties

Elements	Serial properties
r_m, vasculature root	*RL* (r_m), root label
	RSL (r_m), connected branches, as sub-trees
s_i, vessel segments	VL (s_i), branch label
	VLen (s_i), branch length
	VRad (s_i), mean radius of vessel branch
	VLV (s_i),branch level
	VR (s_i), associated root label
	VP (s_i), associated connection points' labels
	VT (s_i), associated sub-tree label
b_j, bifurcations	*BL* (b_j), connection point label
	BV (b_j), associated branches' labels
e_k, extremities	*EL* (e_k), extremities label
	ELR (e_k), length from root to extremity
	EB (e_k), associated branch

refers to points having more than two 26-connected neighbours. Each segment is assigned with a unique label. Then, all the intersection points are isolated and morphologically dilated by a $3 \times 3 \times 3$ structure element. Each component is considered, and labelled, as a bifurcation of the vasculature. Finally, tree roots are dilated to overlap the vessel segment connected to the root. These segments are considered as root segment which are assigned the tree level $VLV(s_i) = 1$, the associated root label $VR(s_i)$ and a sub-tree labels $VT(s_i)$.

Finally, some properties listed in last section can be accumulated before the tree growing process. The branch length $VLen(s_i)$ is assessed by the path from one extremity to the other. The distance between two neighbour voxels is Euclidean distance 1, $\sqrt{2}$ or $\sqrt{3}$ in terms of the connection type, including face-connected, edge-connected or vertex-connected, respectively. The associated connection points $VP(s_i)$ are the overlap bifurcations. Each voxel of individual segment is regards as the centre of the maximal inscribed sphere of the vasculature. Therefore, the mean radius of a vessel $VRad(s_i)$ is computed using the radius of all these maximal inscribed sphere.

The graph-based watershed methodology [20] is used to associate isolated vessel segments to grow vascular tree. Typically, the watershed method is applied for image analysis-based pixels which are named as nodes and seeds. In this case, the nodes are the individual vessel segments instead of pixels and seeds are the root segments. Root segments are initially put in a priority queue. Vessel segments are repeatedly taken from the top of the queue, and its neighbouring vessel segments are added with priority of mean radius $VRad(s_i)$. Radius is used to determine the priority as it is the reasonable indicator of the tree hierarchy. Once a segment is taken out of the queue, it passes the properties to its neighbours being never added into the queue. Accordingly, the segments inherit the associated root $VR(s_i)$ and the sub-tree label $VT(s_i)$. The same branch level $VLV(s_i)$ is assigned to the segment with the highest priority, while a higher level to the others. Meanwhile, the length to the root is accumulated at this stage. The process that segments are passed in and out of the queue terminates until all the segments are removed out of the queue.

3.3.4 The quantification output

The quantification result is presented in both statistics and image patterns. The image-wide summary of vasculature includes the following statistics:

- Number of roots—number of vascular tree
- The total length of all the vascular branches (in pixels)
- Total number of vascular segments
- The longest length extended from the root
- Total number of extreme vessels
- Total number of branch points.

For the tree structure-based quantification, the statistics are grouped in terms of sub-tree label. Each sub-tree contains following measurement:

- Tree label
- Total length of the tree
- Length of longest vessel from the root
- Max branch layer
- Mean branch layer
- Number of branch points
- Number of vessel segments
- Number of extreme vessels.

The length and mean radius of the individual vessel segment are output in a list. Two images produced to present the vascular tree intuitively are shown in Fig. 5. One is vessel trees, in which the vessel branches are of grey values according to its sub-tree label. This image presents different trees in whole. The other one is the branch level image. It shows the hierarchy of the vasculature with different grey values in terms of the branch level.

4 Quantification results

A series of mouse liver images are used to evaluate the proposed quantification method of tree analysis. The images are grouped according to different stage of hepatic fibrosis. There are 8 set of images for mouse livers in total, including three normal livers, three sets at mild stage of hepatic fibrosis and two sets at advanced stage. In order to achieve statistical significance, we truncated the images of relatively intact samples to obtain more images, which

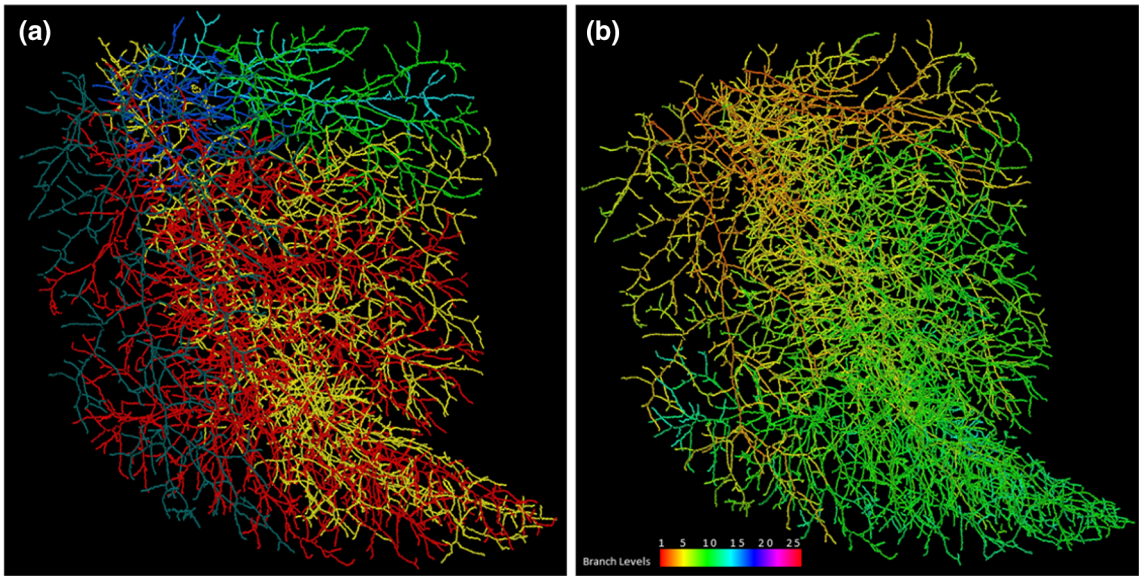

Fig. 5 Visualization of vascular tree structure by output images. **a** Vessel trees; **b** branch levels

simulate the incomplete or non-intact samples. First, the longest axis is found inside each sample's convex volume. The orthogonal plane at one-third of the axis is used to remove some part of the liver samples. One non-intact sample is generated from samples called "NA", "NB", "3A" and "mouse2", respectively. In advanced group, the sample "mouse3" generated two non-intact samples, and the existing non-intact sample "mouse5" removes one-fourth of its tissue to generate worse non-intact samples. Therefore, there are 5 samples in each fibrotic group, which are enough to demonstrate the statistical significance to some extent. They are quantified according to the tree analysis workflows described in the section above. As an example, the images for the tree analysis of one normal mouse liver (Sample "NB") are given in Fig. 6.

Figure 6b is the segmentation result of the vasculature, and Fig. 6c is its skeleton. They are the critical intermediate step of our quantification method. Figure 6d, e are the final output images of proposed tree analysis, which intuitive display of the vasculatures in hierarchy. Corresponding statistics of the liver "NB" are listed in Table 2.

The data in Table 2 tend to be too abstract to study the hepatic fibrosis. To evaluate the level of angiogenesis for the investigation of hepatic fibrosis or other vasculature-related diseases, the fractional volume and densities of vascular segments, terminal vessel branches and bifurcations are usually used [21, 22]. These parameters are employed in our analysis to all the three sample groups. These densities, described by the volume used for density evaluation, are computed by integrating the convex hull of the vasculature. The correspondent results are shown in Fig. 7.

According to the density values given in Fig. 7, only the average value of segment density shows obvious increasing trend (106.4, 121.0 and 142.4 for samples at normal, mild and advanced levels of fibrosis, respectively), while those for the extremities and branch points do not follow this regularity of fibrotic progression. Abnormal values could be found in the charts, such as the density for sample "NA" and "3A". In addition, the large standard deviations in Fig. 7 show obvious fluctuation of density value among samples in the same group, implying that a normalized parameter should be defined to evaluate the level of fibrosis more accurately.

The angiogenesis is a prominent characteristics of hepatic fibrosis [22]. It is a process that vasculature rapidly proliferates. The vessel segments outgrow from existing vessels [23], and the newly generated vessels normally occupy higher levels of the vascular tree. Thus, the mean level of a vascular tree increases as the angiogenesis develops. The indicator for branch level is normalized so that it can be used in statistics. To evaluate the level of angiogenesis, a new parameter called high-level vascular ratio is defined as HVR = average level/maximum level, where the average level denotes the mean level of a single vascular tree and the maximum level is the highest level of the same tree.

The HVR is extracted from the level quantification of the vascular tree. The parameter is defined based on a typical kind of vascular tree so that criterion for comparison among samples can be standardized. As well known, most of liver blood flow is through the hepatic portal vein, vasculature of which contains the thickest vessel segment in the liver tissues. The hepatic portal vein is characterized in terms of the vessel radius and the branch level in vasculature trees. Therefore, the hepatic portal vein of each specimen is identified from the quantitative parameters, including mean radius of vessel segment and branch level. For a compromise between accuracy and efficiency, branch

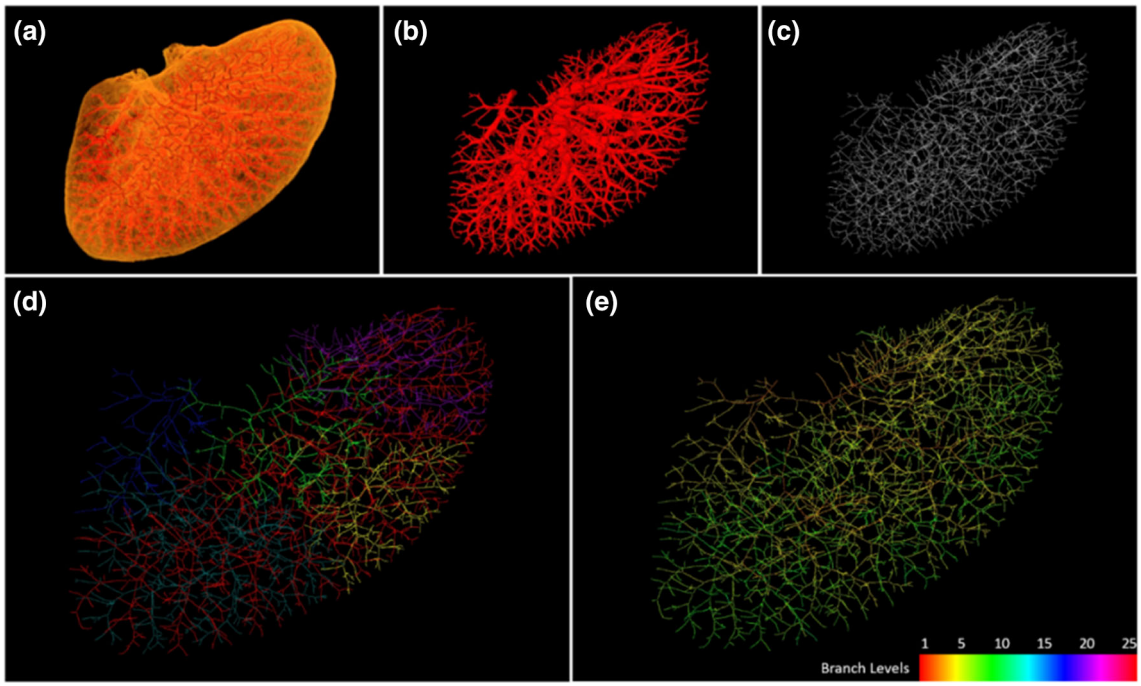

Fig. 6 Quantification for a normal mouse liver: **a** raw image, **b** the vasculature, **c** the vascular skeleton, **d** vascular trees of the liver and **e** the branch levels of all vessel segments

Table 2 Statistics for a normal mouse liver (sample "NB")

Sample name	Total length	Total number of vascular segments	Tile longest vessel	Total number of extreme vessels	Total number of branch points
Quantification of image-wide vasculature (The length measurement is in pixel unit)					
NB	67,885.4	3317	741.736	1697	1507

Tree label	Total length	Longest vessel	Max level	Mean level	Total number of branch points	Total number of vascular segments	Total number of extreme vessels
Statistics of each vascular tree							
1	8424.48	482.28	8	4.14	180	399	204
2	31,171.4	741.74	11	6.14	691	1512	771
3	7292.82	525.41	7	3.67	167	374	195
4	5620.86	347.04	7	3.21	130	280	143
5	3099.46	390.63	6	3.31	61	139	71
6	12,276.3	552.17	9	4.36	278	613	313

level of 5 for the vessel segments is usually large enough to identify the hepatic portal vein. Figure 8 shows the *HVR* value of each hepatic portal vein in all samples. The *HVR* correctly reflects the trend of angiogenesis when the degree of hepatic fibrosis aggravates, the larger the *HVR* value is, the higher the angiogenesis level. For samples in the same group in Fig. 8, the fluctuation of *HVR* value is greatly reduced compared to the conventional density parameters in Fig. 7. This means that the proposed *HVR* parameter can be used to evaluate the degree of fibrosis accurately. Among all the samples, most of the vasculatures used for the quantitative analysis are not intact, implying that the *HVR* parameter is robust even if a specimen misses a portion of vasculature.

5 Discussion

The segment or bifurcation density is usually adopted to evaluate the degree of hepatic fibrosis in some cases. However, these parameters do not always work and may lead to incorrect assessment results, in cases that the three-

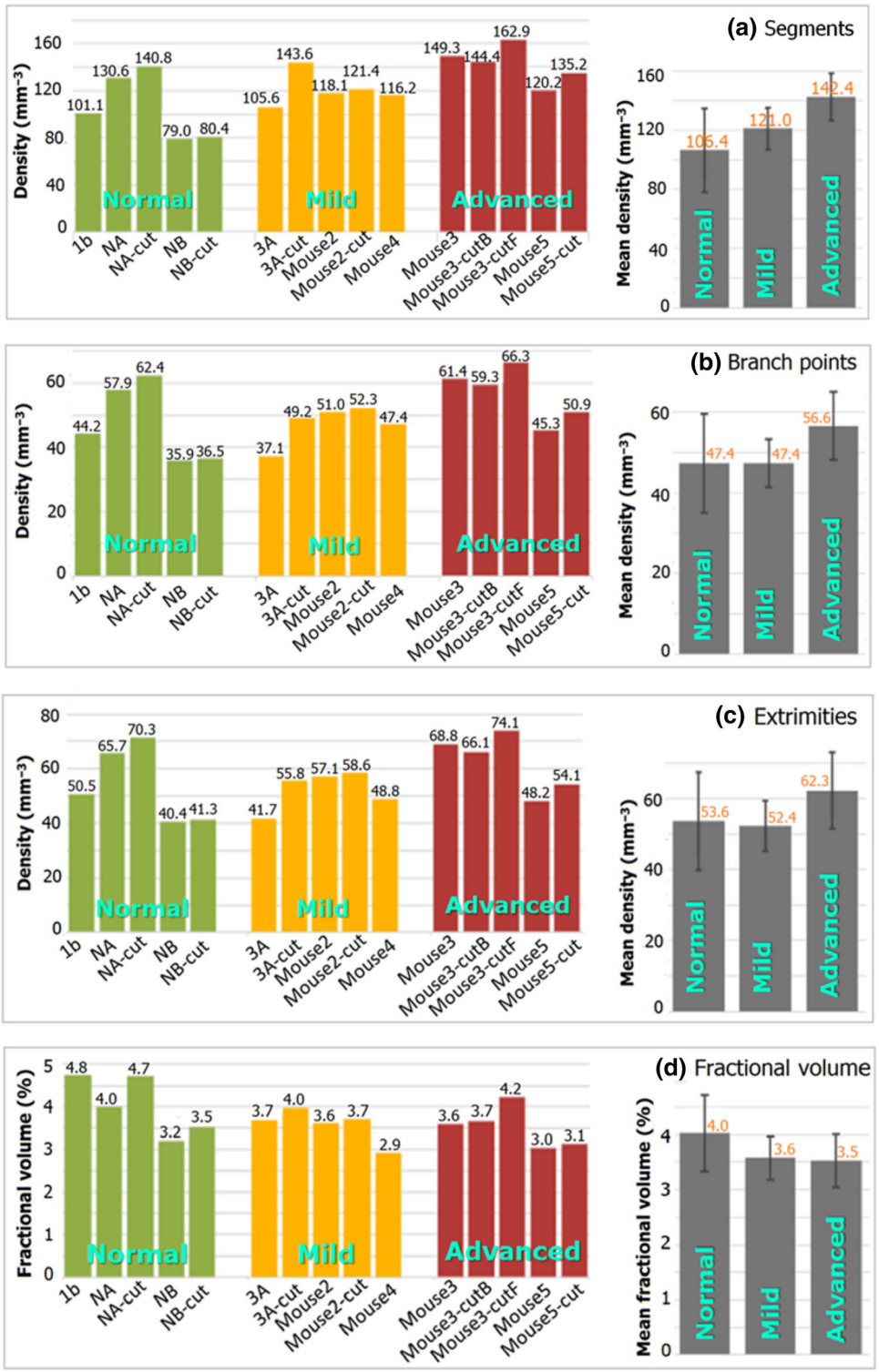

Fig. 7 Common use indices of evaluating angiogenesis for all specimens. **a** Micro-vessel density (MVD), **b** ratio of junction point to volume (*J*/*V*), **c** ratio of extremities to volume, **d** fractional volume

dimensional vasculature of the samples is not imperfect due to factors in sample preparation or image collection. The experimental results demonstrate that the proposed parameter *HVR* is robust and reliable in the evaluation of the angiogenesis, compared to those commonly used density measurements. As the vessel segments are not uniformly distributed inside a liver, the density measurements relying on the segment number and the vascular convex volume may vary significantly in different liver regions. With the proposed measurement in this paper, the tree analysis of hepatic portal vein for each specimen shows that the new measurement can obtain a robust and

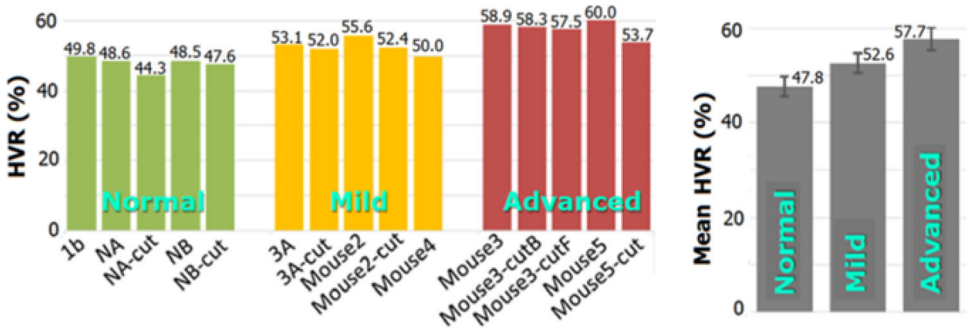

Fig. 8 *HVR* of each hepatic portal vein inside the liver samples

reliable trend of the angiogenesis development which accurately reflects the degree of hepatic fibrosis. Therefore, we can conclude that the proposed method is practical for the evaluation of the angiogenesis, despite all kinds of image data imperfections. The proposed method can also be extended to investigate other diseases in which vasculature change is a key indicator, such as tumour in the period of formation and growth, and cardiovascular diseases.

References

1. R. Bataller, D.A. Brenner, Liver fibrosis. J. Clin. Invest. **115**, 209–218 (2005). doi:10.1172/JCI24282
2. D. Schuppan, N.H. Afdhal, Liver cirrhosis. Lancet **371**, 838–851 (2008). doi:10.1016/S0140-6736(08)60383-9
3. Q.T. Lemos, Z.A. Andrade, Angiogenesis and experimental hepatic fibrosis. Mem. Inst. Oswaldo Cruz **105**, 611–614 (2010). doi:10.1590/S0074-02762010000500002
4. D.D. Hu, Y. Chen, A. Bihi et al., A new conversation between radiology and pathology-identifying microvascular architecture in stages of cirrhosis via diffraction enhanced imaging in vitro. PLoS ONE **9**, e87957 (2014). doi:10.1371/journal.pone.0087957
5. R. Chen, P. Liu, T. Xiao et al., X-ray imaging for non-destructive microstructure analysis at SSRF. Adv. Mater. **26**, 7688–7691 (2014). doi:10.1002/adma.201402956
6. S. Bonekamp, I. Kamel, S. Solga et al., Can imaging modalities diagnose and stage hepatic fibrosis and cirrhosis accurately? J. Hepatol. **50**, 17–35 (2009). doi:10.1016/j.jhep.2008.10.016
7. J.H. Duan, C.H. Hu, S.Q. Luo et al., Microcomputed tomography with diffraction-enhanced imaging for morphologic characterization and quantitative evaluation of microvessel of hepatic fibrosis in rats. PLoS ONE **8**, e78176 (2013). doi:10.1371/journal.pone.0078176
8. S. Kaur, K. Anita, Angiogenesis in liver regeneration and fibrosis: "a double-edged sword". Hepatol. Int. **7**, 959–968 (2013). doi:10.1007/s12072-013-9483-7
9. Y. Fu, H. Peng, X. Zhang et al., Assessment of fibrotic tissue and microvascular architecture by in-line phase-contrast imaging in a mouse model of liver fibrosis. Eur. Radiol. **26**, 2947–2955 (2016). doi:10.1007/s00330-015-4173-6
10. P. Bedossa, T. Poynard, An algorithm for the grading of activity in chronic hepatitis C. Hepatology **24**, 289–293 (1996). doi:10.1002/hep.510240201
11. M.H. Ismail, M. Pinzani, Reversal of hepatic fibrosis: pathophysiological basis of antifibrotic therapies. Hepat. Med. **3**, 69–80 (2011). doi:10.2147/HMER.S9051
12. H. Xie, B. Deng, Y. Fu et al., Latest advances of X-ray imaging and biomedical applications beamline at SSRF. Nucl. Sci. Tech. **26**, 20102 (2015). doi:10.13538/j.1001-8042/nst.26.020102
13. R. Chen, D. Dreossi, L. Mancini et al., PITRE: software for phase-sensitive X-ray image processing and tomography reconstruction. J. Synchrotron Radiat. **19**, 836–845 (2012). doi:10.1107/S0909049512029731
14. S. Bolte, F.P. CordelièRes, A guided tour into subcellular colocalization analysis in light microscopy. J. Microsc. **224**, 213–232 (2006). doi:10.1111/j.1365-2818.2006.01706.x
15. N.D. Cornea, D. Silver, P. Min, Curve-skeleton properties, applications, and algorithms. IEEE Trans. Vis. Comput. Graph. **13**, 530–548 (2007). doi:10.1109/Tvcg.2007.1002
16. T.C. Lee, R.L. Kashyap, C.N. Chu, Building skeleton models via 3-D medial surface axis thinning algorithms. Graph. Models Image Process. **56**, 462–478 (1994). doi:10.1006/cgip.1994.1042
17. H. Homann, Implementation of a 3D thinning algorithm. Insight J. (2007). http://hdl.handle.net/1926/1292
18. D. Shaked, A.M. Bruckstein, Pruning medial axes. Comput. Vis. Image Underst. **69**, 156–169 (1998). doi:10.1006/cviu.1997.0598
19. D. Wang, R. Lagerstrom, C. Sun et al., HCA-vision: automated neurite outgrowth analysis. J. Biomol. Screen. **15**, 1165–1170 (2010). doi:10.1177/1087057110382894
20. R. Lagerstrom, M. Buckley, A graph watershed method for analysis and quantification of neurite branching structure, in *Proceedings of the 18th World IMACS/MODSIM Congress*, Cairns, Australia, 2009, 762–767
21. C. Paternostro, E. David, E. Novo et al., Hypoxia, angiogenesis and liver fibrogenesis in the progression of chronic liver diseases. World J. Gastroenterol. **16**, 281–288 (2010). doi:10.3748/wjg.v16.i3.281
22. C. Bocca, E. Novo, A. Miglietta et al., Angiogenesis and fibrogenesis in chronic liver diseases. CMGH **1**, 477–488 (2015). doi:10.1016/j.jcmgh.2015.06.011
23. A. Birbrair, T. Zhang, Z.-M. Wang et al., Pericytes at the intersection between tissue regeneration and pathology. Clin. Sci. **128**, 81–93 (2015). doi:10.1042/cs20140278